Journal of
Synchrotron
Radiation

ISSN 0909-0495

Received 10 December 2004
Accepted 22 March 2005

X-ray spectroscopy and X-ray diffraction at wavelengths near the *K*-absorption edge of phosphorus

Valérie Biou,[a] Peter Bösecke,[b] Jean-Marie Bois,[c] Gérard Brandolin,[d] Richard Kahn,[e] Corinne Mas,[d] Lionel Nauton,[e] Hugues Nury,[e] Eva Pebay-Peyroula,[e] Jean Vicat[e] and Heinrich Stuhrmann[e,f]*

[a]Laboratoire d'Enzymologie et de Biochimie Structurales CNRS, Avenue de la Terrasse, 91198 Gif sur Yvette CEDEX, France, [b]ESRF, BP 220, 38043 Grenoble CEDEX 9, France, [c]EMBL Grenoble Outstation, c/o ILL, BP 156, 38042 Grenoble CEDEX 9, France, [d]Laboratoire de Biochimie et Biophysique des Systèmes Intégrés, UMR 5092, CEA/CNRS/UJF, Département de Réponse et Dynamique Cellulaires, CEA-Grenoble, 17 Avenue des Martyrs, F-38054 Grenoble, France, [e]Institut de Biologie Structurale Jean-Pierre Ebel, CEA/CNRS/UJF, UMR 5075, 41 rue Jules Horowitz, F-38027 Grenoble CEDEX 1, France, and [f]GKSS Forschungszentrum, D-21502 Geesthacht, Germany. E-mail: stuhrmann@ibs.fr

Phosphorus is an abundant element in living organisms. It is traceable by its X-ray absorption spectrum which shows a strong white line at its *K*-edge, comparable with that observed for the L_{III} edges of rare earth ions. With purple membrane, the variation of the imaginary part of the anomalous dispersion of phosphorus is found to be close to 20 anomalous electron units. Anomalous diffraction experiments at wavelengths near the *K*-absorption edge of phosphorus confirm this result. The spatial distribution of lipids derived from anomalous diffraction agrees with earlier results from neutron diffraction. Test experiments on single crystals of the carrier protein using 5.76 Å photons gave a first low-resolution diffraction pattern. Various techniques of crystal mounting were attempted. In addition, fluorescence measurements on a solution of threonine synthase appear to hint at a change of the phosphate environment of the cofactor upon activator binding.

Keywords: phosphorus *K*-edge; purple membrane; ADP/ATP carrier protein; fluorescence; anomalous diffraction.

1. Introduction

Phosphorus is present in all living cells: membrane phospholipids, ribonucleotides such as DNA, RNA or ATP, and also in other essential compounds such as pyridoxal phosphate (vitamin B6). It is therefore useful to be able to probe phosphorus with X-rays. Unlike sulfur, which can be substituted by selenium in quite a number of cases, phosphorus is not amenable to substitution by its heavier homologue, arsenic. Structural studies on macromolecules have to rely on phosphorus as such. Examples are the soft X-ray contact microscopy techniques developed by Ito *et al.* (1998, 2003), allowing analysis of localization and chemical status of minor elements (Ca, S, P *etc.*) in biological specimens at relatively spatial resolution compared with X-ray diffraction. The technique of multiwavelength anomalous diffraction (MAD) relying on X-ray diffraction at wavelengths near the *K*-edge of phosphorus turns this element into a native label of macromolecular crystallography. In spectroscopic techniques, phosphorus is a useful local probe.

Because of the technical difficulties (see §2.1) owing to their low energy, X-ray diffraction experiments at wavelengths near the *K*-absorption edge of phosphorus (λ_K = 5.76 Å corresponding to E = 2151 eV) have been rather rare. Indeed, soft X-ray studies present even more challenges than softer X-rays (see companion paper in this issue, Djinović Carugo *et al.*, 2005). The first test experiments on purple membrane were carried out by Munk (1988*a*). An anomalous diffraction study on single crystals of the small subunit of ribosomes from *Thermus thermophilus* at wavelengths near the *K*-edge of phosphorus seems to be the first to be reported (Stuhrmann *et al.*, 1995). In 2000, M.-L. Chesne showed that single crystals of lysozyme diffract X-rays with photon energies down to E = 2.17 keV (λ = 5.7 Å) (Chesne, 2002; Carpentier *et al.*, 2002).

Phosphorus in phosphates gives rise to a strong peak (a so-called white line) at its *K*-absorption edge (George *et al.*, 1993). As will be shown below, the strong anomalous change (or anomalous dispersion) of X-ray absorption reflects a change in the atomic scattering amplitude, which compares with that of the rare-earth ions at their L_{III}-

absorption edges. Phosphorus in living matter thus becomes a native label of impressive strength once the wavelength of the primary beam is tuned to a wavelength close to its *K*-absorption edge.

Previous attempts of soft X-ray diffraction from proteins (Lehmann *et al.*, 1993; Stuhrmann *et al.*, 1997; Carpentier *et al.*, 2002) have led to the design of a helium-filled cylindrical box that meets the requirements of both spectroscopy and diffraction of soft X-rays. The first part of this paper will outline the concept of the X-ray detection system and its realisation at the beamline ID01 of ESRF, Grenoble, France. The performance of this special-purpose device complementing ID01 will be illustrated by test experiments of fluorescence and/or diffraction from purple membrane stacks, threonine synthase solutions and single crystals of ADP/ATP carrier protein.

2. Instrument design for soft X-ray diffraction and soft X-ray spectroscopy

2.1. Technical challenge

The penetration depth (*i.e.* 1/e absorption pathlength) of soft X-rays is relatively small in almost any material. This is illustrated in Table 1 for some materials relevant to experiments at wavelengths near the *K*-edge of phosphorus.

As open-air X-ray diffractometers would not be suitable for soft X-ray diffraction, two solutions for the reduction of absorption may be envisaged:

(i) The X-ray path is evacuated. An air gap of a couple of millimetres is allowed around the sample (Stuhrmann *et al.*, 1997);

(ii) The X-rays pass through a helium atmosphere. The sample is frozen by a cold helium stream (Carpentier *et al.*, 2002).

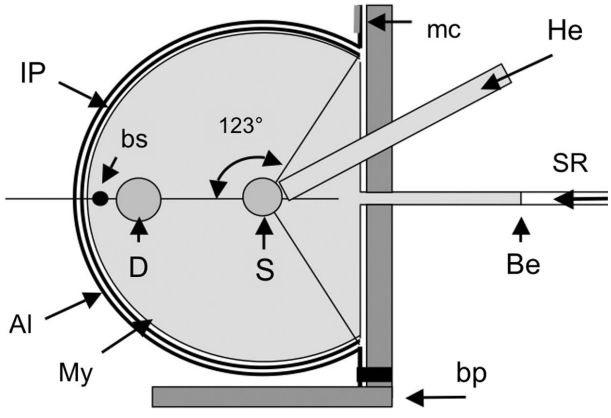

Figure 1
Side view of the helium box. Synchrotron radiation (SR) reaches the sample (S) at the centre of the cylinder from the right-hand side of the figure through a beryllium window of thickness 25 µm (Be). The image plate (IP) covers two-thirds of a cylinder jacket, the maximum scattering angles being ±123°. A thin aluminium plate (Al) holds it. The upper edge of the Al plate is fixed to the base plate (bp) by a magnetic clasp (mc). The large Mylar window (My) of the helium box has a thickness of 6 µm. The entrance D is used for the fixation of various devices (*e.g.* for the fluorescence detector). A rod of diameter 3 mm serves as beam stop (bs).

Table 1
Penetration depth of soft X-rays, at the *K*-edge of phosphorus (room temperature).

Material	Penetration depth
Water, polymers (*e.g.* polyethylene terephthalate, used for Mylar foils)	20 µm
Beryllium	70 µm
Air	2.0 cm
Helium	3.5 m

The helium atmosphere is preferred as it is easier to maintain. It is essentially transparent to soft X-rays and it allows direct cooling of the protein crystal. At temperatures $T \leq 100$ K, radiation damage to protein crystals is known to be much less severe than at room temperature.

The structural resolution given by $d = \lambda/(2\sin\theta)$ decreases with longer X-ray wavelengths, λ. This drawback can in part be compensated for by allowing for a larger range of the scattering angle 2θ. For $\lambda = 5.76$ Å the best structural resolution of 2.88 Å is achieved at $2\theta = 180°$ (back reflection). With a diffraction data set extending to $2\theta = 60°$, the structural resolution limit is equal to the wavelength used, *i.e.* 5.76 Å. Hence, there is a strong need to extend diffraction data collection to large angles in order to reach a reasonably high completeness of diffraction data, say within 3 Å resolution. The use of a detector covering a large solid angle is therefore mandatory. In practice, a cylindrical area detector is a good choice, ideally combined with a goniostat to allow a second setting of the crystal orientation for low-crystal-symmetry cases.

2.2. Technical realisation of the helium box

2.2.1. Cylindrical box and the cryogenics. Following the above constraints, a helium box has been designed for implementation into the diffractometer of beamline ID01 at the ESRF. It is cylindrical in shape (Figs. 1 and 2). The axis of the cylinder in the horizontal direction coincides with the φ-axis of the diffractometer (Fig. 2). A bent image plate (355 mm × 435 mm) covers two-thirds of the cylinder jacket

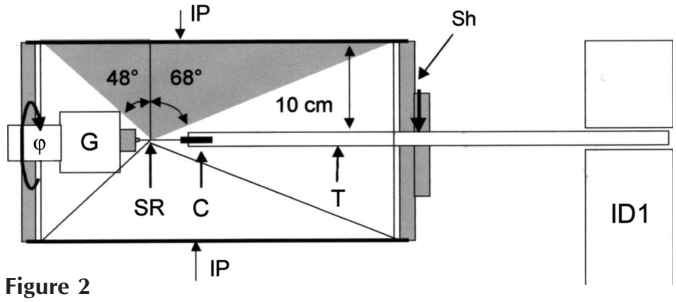

Figure 2
View towards the synchrotron radiation source (SR) of the helium box and its transfer line. The image plate (IP) covers scattering angles from −48° to +68°. The angular asymmetry is not intentional but due to constraints which existed at ID01 until recently. Now the angular range is ±63°. The sample cell held by the guide tube (T) is docked to the goniometer head (G). When the tube leaves the helium box the shutter (Sh) will close automatically. An axial movement of ±14 mm of the helium box is remote controlled.

(Fig. 1). Synchrotron radiation and the helium gas enter the helium box from the same side (right-hand side in Fig. 1). In the absence of the sample, the 5.76 Å photons selected by the double-mirror double-monochromator system of beamline ID01 are attenuated by 25 μm beryllium, 30 cm helium and 6 μm Mylar foil. Under these conditions, 48% of the incident monochromatic radiation is transmitted to the detector.

As has already been mentioned above, the use of cold helium gas, typically at temperatures $T \leq 100$ K, is needed to preserve biological samples, and protein crystals in particular. Cold helium gas is obtained with the Oxford Cryo-System 700 using a slightly modified procedure. The low temperature inside the helium box requires several precautions. As the large Mylar window becomes very cold, a layer of frost is formed on its outer surface within a few seconds, rendering the window opaque to soft X-rays and more vulnerable to mechanical stress. To avoid this, the window is kept warm by using an electrically heated aluminium cover plate. During exchange of the image plate, a dry-nitrogen fan reduces the frost formation to a good extent when the warm aluminium cover plate is opened,

2.2.2. Handling of the samples. Protein solutions were deposited on a Mylar foil and allowed to partially dehydrate in air for about 30 min before mounting. Protein crystals were mounted on a loop, as commonly used today, or on a thin plastic foil.

The samples were introduced into the cold helium atmosphere by using a newly developed sample transfer line (Fig. 2). The transfer line is most useful for frozen protein crystals. The sample, while being moved along the cylinder axis, remains at $T < 100$ K owing to the presence of a small amount of liquid nitrogen in the cell. After mounting the sample on the goniometer head, the residual dry nitrogen will escape into the helium atmosphere of the box. It is removed by the continuous helium flow. As the access of air is prevented, no frost is formed inside the helium box. Exchange of the sample is easy and reliable, and takes barely more than 10 s.

2.2.3. Detectors used. Fluorescence is measured by a detector (XR100CR from AmpTek, 25 mm^2 sensitive area, 25 μm beryllium window) facing the sample in the direction of the cylinder axis, *i.e.* at 90° with respect to the incident beam. It is retracted from this position when the sample is exchanged or when X-ray diffraction is measured. The fluorescence detector remains resident in the helium box.

X-ray diffraction is measured using a flexible image plate particularly sensitive to low-energy radiation (unmounted low-energy storage phosphor screen from Amersham Biosciences). Its size is slightly larger than the scanned area of 355 mm × 435 mm. The image plate is pressed against the Mylar window by a thin aluminium plate and is thus cylindrically bent (Fig. 1). Lights are switched off during the measurement of the diffracted intensity and the plate is transported from the helium box to the scanner inside an opaque cover. The image plate is read out off-line.

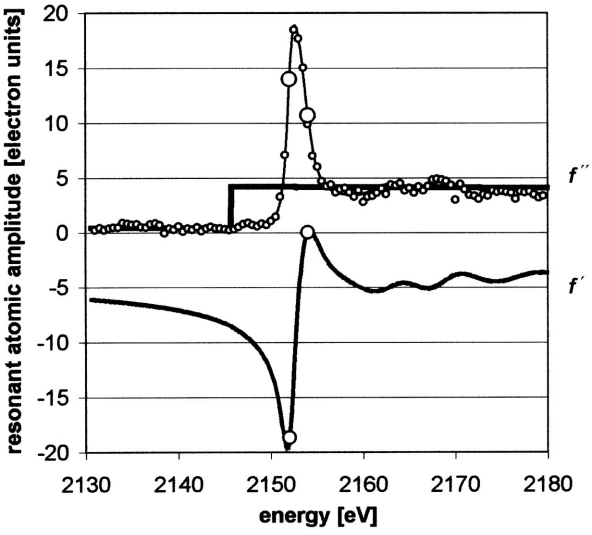

Figure 3
Anomalous dispersion of phosphorus from the phospholipids of purple membrane at energies near the *K*-edge. Circles denote the imaginary part, f''. The real part, f' (line), is negative, except at 2154 eV where it is close to zero. The large circles denote the wavelengths used in anomalous diffraction from purple membrane.

3. Results from purple membrane

Purple membrane has been the subject of numerous studies. While the structure of its membrane protein bacteriorhodopsin is well known (Henderson & Unwin, 1975; Henderson *et al.*, 1990; Belrhali *et al.*, 1999), this is much less the case with the lipid phase. The latter is rich in phosphates and sulfates. The anomalous signal of both phosphorus and sulfur may therefore facilitate a description of the lipid–protein interaction. The results from a first study using the anomalous dispersion of phosphorus in purple membrane are reported below.

3.1. Phosphorus is a strong anomalous scatterer

The fluorescence intensity from a stack of purple membrane near the *K*-edge of phosphorus was measured at $T = 100$ K. The data were scaled to the anomalous dispersion curves published by Henke *et al.* (1993). The imaginary part f'' of the anomalous dispersion varied by 20 electron units near the *K*-absorption edge (Fig. 3). The change of the real part f' was similar in amplitude. Note also that there was a shift of the *K*-edge of phosphate (see Table 2) with respect to elemental phosphorus by about 8 eV (George *et al.*, 1993). A similar result was obtained from anomalous small-angle X-ray scattering of the large sub-unit of *E. coli* ribosomes (Hütsch, 1992; Stuhrmann, 1994). Anomalous dispersion near the *K*-edge makes phosphorus an excellent native label in structural studies.

3.2. Anomalous X-ray powder diffraction from purple membrane

The purple membrane of *Halobacterium halobium* consists of about 25% lipid and 75% protein, and the protein is thought to be a single species, bacteriorhodopsin. Samples of

Table 2
Chemical composition of the lipid phase of purple membrane [data from Jost *et al.* (1978)].

	P	S	No. of P atoms per protein molecule	No. of S atoms per protein molecule
Phosphatidyl glycerol	1	0	0.14	0
Phosphatidyl glycerophosphate	2	0	13.28	0
Phosphatidyl glycerosulfate	1	1	0.69	0.69
Glycolipid sulfate	0	1	0	1.24
Total membrane			14.1	1.9

purple membrane are most suitable for exploring anomalous diffraction using soft X-rays. The thickness of the membrane stack deposited on a 10 μm Mylar foil is easily adjusted to a penetration depth of 20 μm at wavelengths near the *K*-edge of phosphorus. It is presumed that the plane of the membrane stack is orthogonal to the incident beam. The powder diffraction in Fig. 4 was obtained in 20 min at ID01 using the helium box shown in Fig. 1. The powder rings are well separated and most of them are assigned to single doublet indices (h,k), typical for a two-dimensional lattice. This prominent in-plane diffraction (Fig. 4) indicates that the proteins and the lipids are regularly packed in a hexagonal array in the plane of the membrane. The plane group of the two-dimensional lattice is *p*3. The dry sample, which had been prepared in 1993, the diffraction pattern of which had remained unchanged since then, has a lattice constant $a = 61$ Å.

Anomalous X-ray diffraction at wavelengths near the *K*-edge of phosphorus is a way of obtaining structural information on the phospholipids of purple membrane. The intensity of a given reflection is given by the following expression,

$$I = |U|^2 + 2f' \,\mathrm{Re}\,(UV^*) + \left(f'^2 + f''^2\right)|V|^2,$$

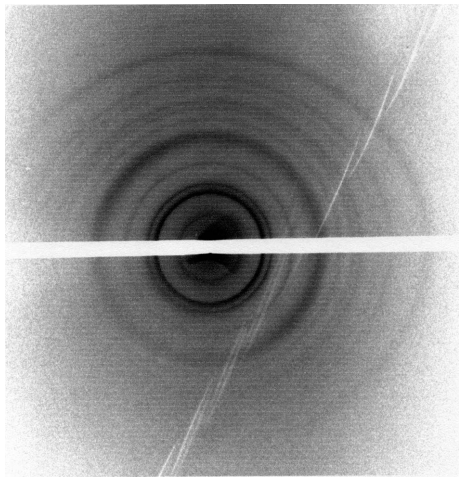

Figure 4
Diffraction of 5.76 Å photons from purple membrane. The white stripes are due to folds of the Mylar foil. Such a fold typically increases the effective thickness of the window by a factor of three, *i.e.* from 6 μm to 18 μm. The reduction in transmission of soft X-rays by just 12 μm more plastic foil is impressive.

where U is the structure factor in the absence of anomalous dispersion and V is the structure factor of those atoms whose anomalous dispersion is considered to be relevant. The intensity, I, varies mainly with the real part f' of anomalous dispersion, whereas the term proportional to f'' vanishes owing to the symmetry of the phospholipid double layer.

For a purple membrane stack, strong anomalous diffraction is expected near the absorption edge only. Hence, the intensity of X-ray diffraction was measured at $E_1 = 2152$ eV and $E_2 = 2154$ eV, where the difference in f' is largest and the change in absorption (proportional to f'') is small (Fig. 3).

Significant changes in the diffracted intensity are observed for the low values of (h,k) (Fig. 5), notably with the (2,0) and (1,1) reflections and to a smaller degree with the (2,1) reflection. This result agrees remarkably well with corresponding neutron diffraction data from purple membrane in H_2O/D_2O mixtures (Worcester, 1975; Saibil *et al.*, 1976; Zaccai & Gilmore, 1979; Chabre *et al.*, 2003). Anomalous dispersion of X-ray diffraction from phosphorus in the phospholipids plays the same role as isotopic substitution of hydrogen isotopes in neutron scattering (Figs. 6*a* and 6*b*). While for contrast variation by neutron scattering the preparation of several samples in different H_2O/D_2O mixtures was necessary, that for anomalous X-ray diffraction requires a single sample at two wavelengths near the *K*-absorption edge of phosphorus (Fig. 3).

As the phases of the structure factors (h,k) are known (Seiff *et al.*, 1985), the spatial distribution of the phosphorus atom in the hexagonal unit cell is obtained from the difference Fourier electron density map (Fig. 7). Phosphorus, as part of the polar heads of the phospholipids, occupies the space between the proteins (Fig. 8), as does water (Worcester, 1975). Both provide a negative print of the hexagonal protein lattice. A quantitative analysis of the intensity change owing to anomalous dispersion relies on knowledge of the chemical composition of the lipid phase of purple membrane (Table 2).

For the (1,1) and (2,0) reflections, there is a change in the intensity of X-ray scattering by 20 (±2)% on going from $E_1 =$

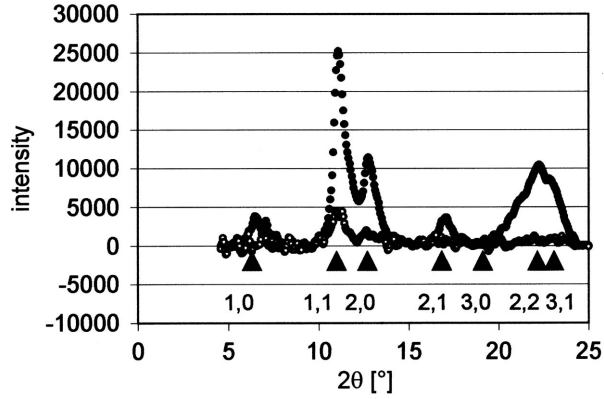

Figure 5
The intensity diffracted by a stack of purple membrane at energy $E_1 =$ 2152 eV (circles) and at $E_2 = 2154$ eV (line) membrane and its difference $I(E_1) - I(E_2)$ (triangles) as a function of scattering angle. Indices (h,k) are marked. The two-dimensional hexagonal plane group is *p*3 with $a = 61$ Å.

2152 eV to E_2 = 2154 eV. This corresponds to a change in their structure factor amplitudes by 10 (±1)%. There are 2200 (±200) excess electrons per monomer protein molecule (M = 26000) with respect to the lipid phase. Hence the increase in contrast on passing from E_2 ($f' = 0$) to E_1 ($f' = -18$ e.u.) is due to 2200 (±200) × 0.1 (±0.01) = 220 (±30) anomalous electron units. The number of phosphorus atoms per monomer protein is 220 (±30)/18 (±2) = 12.2 (±3), in good agreement with the 14.1 phosphorus atoms given in Table 2, reflecting well the chemical composition of the sample.

Note that the anomalous dispersion of the sulfates of the membrane (Table 2) offers an equally valid approach for the study of the lipid–protein interaction in purple membrane (Munk, 1988*b*; Stuhrmann *et al.*, 1991). A comparison between X-ray scattering experiments at wavelengths near the absorption edge of phosphates with those near the *K*-edge of sulfates (λ = 5.0 Å, E = 2480 eV) has been made using data from small-angle scattering of ribosome solutions (Stuhrmann, 1994).

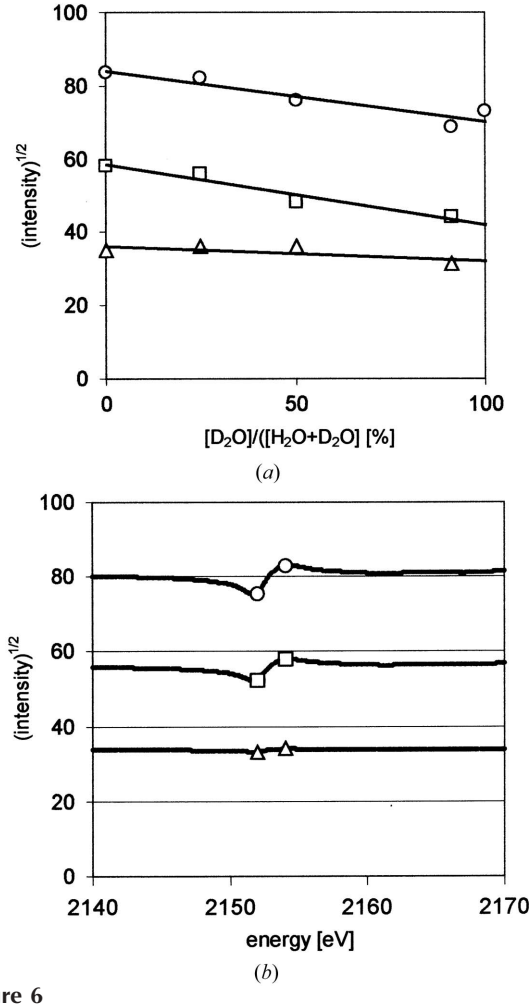

Figure 6
Contrast variation (*a*) in neutron diffraction using H_2O/D_2O mixtures (Worcester, 1975) and (*b*) from anomalous X-ray diffraction. The experimental data are given by the following symbols: circles for the reflection (h,k) = (1,1), squares for (h,k) = (2,0) and triangles for (h,k) = (2,1). Straight lines fit the neutron scattering data. The variation of the X-ray scattering intensity follows the dispersion of f'.

4. Fluorescence measurements on threonine synthase solutions

Threonine synthase (TS) is a pyridoxal phosphate (PLP) dependent enzyme. The study of this enzyme by its fluorescence at the *K*-edge of phosphorus is motivated by two questions. The plant isoform is allosterically activated by S-adenosyl methionine (SAM). Crystal structures of TS (Thomazeau *et al.*, 2001) showed different orientations of the PLP in the active site in the presence or absence of SAM (Mas, Biou & Dumas, in preparation). Would these exist in solution as well? The other question is a technical one. The concentration of phosphorus in the complex is about an order of magnitude lower than with purple membrane. Would the set-up which has been successfully used with purple membrane still give a satisfactory result when the complex is dissolved in water, *i.e.* at concentrations which are almost two orders of magnitude lower than in purple membrane?

Protein solutions at 50 mg ml^{-1}, corresponding to a PLP concentration of 1 mM, were deposited on a Mylar foil and allowed to partially dehydrate in air for about 30 min before mounting. They gave a relatively weak fluorescence at the *K*-

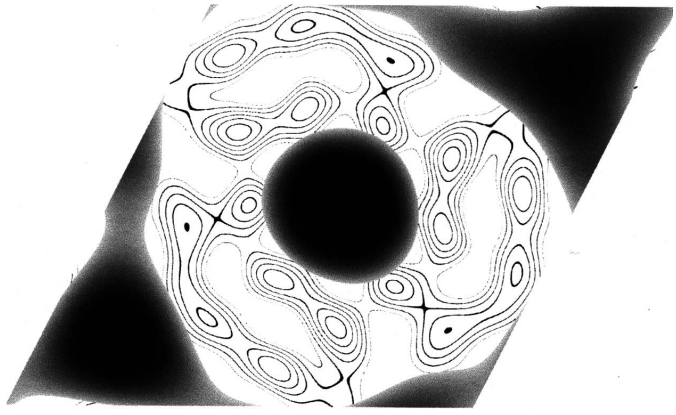

Figure 7
Phospholipid distribution (grey) in the diffraction plane. The difference Fourier map is based on the known structure of bacteriorhodopsin (Seiff *et al.*, 1985) and on the intensity differences from anomalous diffraction of X-rays shown in Figs. 5 and 6. The unit cell contains three bacteriorhodopsin molecules. Their electron density projected on the plane of the membrane is indicated by the contour lines.

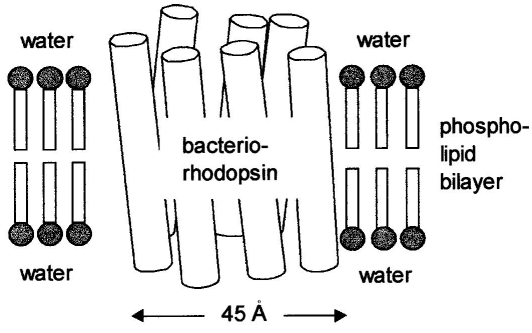

Figure 8
Schematic drawing of purple membrane (after Henderson & Unwin, 1975).

edge of phosphorus at T = 100 K (Fig. 9). By accident the temperature inside the helium box increased. The intensity of the fluorescence doubled when room temperature was reached and it remained constant thereafter. The spectra from both the wet samples (at low temperature) and the dry samples (at room temperature) are shown in Fig. 9.

The spectra taken at low temperature on TS+PLP and TS+PLP+SAM are weaker in intensity and they look quite similar. The difference in intensity between the cold and warm samples is probably due to further dehydration of the sample at room temperature, which increases the protein and PLP concentration. At room temperature, fluorescence spectra show small differences between TS+PLP and TS+PLP+SAM which, if confirmed by further experiments, may arise from changes in the phosphate environment on addition of the activator. We thus have a preliminary confirmation that a change occurs in the PLP environment upon SAM addition.

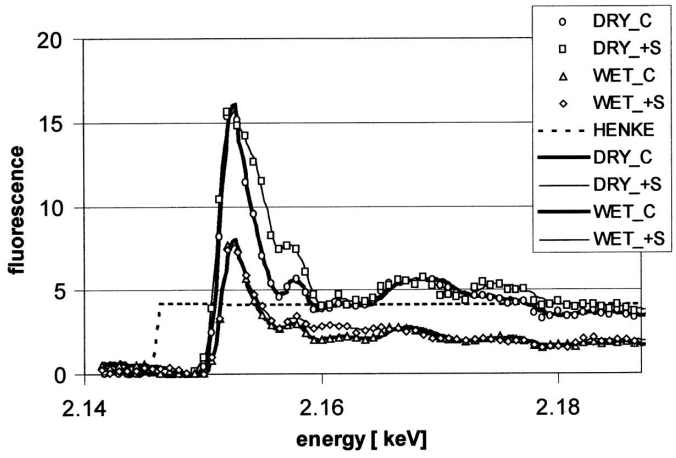

Figure 9
Fluorescence spectra of pyridoxal phosphate-threonine synthase and of the complex activated by S-adenosyl methionine (SAM). Circles: TS + PLP, warm (dry). Squares: TS+PLP+SAM, warm (dry). Triangles: TS+PLP, cold (wet). Diamonds: TS+PLP+SAM, cold (wet).

5. X-ray diffraction of 5.76 Å photons from the ADP/ATP carrier protein

Presently, many efforts are made in the field of structural biology of membrane proteins. Although the results are still limited in number, the information from the high-resolution structures sheds light on important cellular mechanisms such as proton transfer, ion channelling or transport processes. The structural and functional properties of these proteins are highly related to the lipid environment and in particular some individual lipids are tightly interacting with the proteins and play important roles. In the structures present in the Protein Data Bank, some lipids have been described. However, modelling lipid molecules from the electron density maps is not straightforward.

A full description of structure–function relationships in membrane proteins will be achieved if a complete description of bound lipids is facilitated. The possibility of measuring the anomalous signal of phosphor atoms (or sulfur) would help to identify lipids. The ADP/ATP carrier protein, as cardiolipins and phosphatidyl choline lipids, identified from the X-ray structure (Pebay-Peyroula *et al.*, 2003), was chosen as a candidate for first test experiments at wavelengths near the *K*-edge of phosphorus. In a first step it had to be shown whether, and under what conditions, soft X-ray diffraction would be observable.

Crystals from the ADP/ATP carrier protein (Pebay-Peyroula *et al.*, 2003) are obtained as thin platelets. Their thickness is ~5–10 µm, which is about one-third of the 1/e penetration depth of 5.76 Å radiation. Thus, an important condition for obtaining good diffraction images appears to be satisfied. Note that the powder diffraction from purple membrane (Fig. 4) has been obtained from a very small sample, the surface area of which is about 0.5 mm × 0.5 mm = 0.25 mm^2. The surface of a typical single-crystal platelet of the ADP/ATP carrier protein would be 0.1 mm × 0.1 mm = 0.01 mm^2, just 25 times less than with the purple membrane sample and thus probably within reach of present soft X-ray diffraction techniques. An attempt to obtain X-ray diffraction from single crystals of a membrane protein at a wavelength near the *K*-edge of phosphorus was therefore carried out.

Following the example of the purple membrane sample and a protocol developed earlier at HASYLAB (Stuhrmann *et al.*, 1995, 1997), we attempted to mount the carrier protein crystal platelet on a thin Mylar foil, and classically in a cryoloop. The freshly mounted crystals were frozen immediately in liquid nitrogen.

As was observed during an earlier project at HASYLAB (Stuhrmann *et al.*, 1995), only the crystals mounted on a Mylar foil gave diffraction images of usable, albeit variable, quality while those crystals mounted on a loop gave hardly any diffraction peaks. The most successful example obtained with a Mylar foil as support is shown in Fig. 10. The diffraction data have been indexed by assuming a space group $C222_1$ with lattice constants a = 79.9, b = 109.2, c = 89.3 Å (Pebay-Peyroula *et al.*, 2003).

The lesson to be learned is that the art of protein crystallography with soft X-rays begins with the skill invested in crystal mounting. A crystal in a cryoloop is usually covered by a considerable amount of solvent. Soft X-rays will be absorbed in the solvent layer. This apparently has also been the case with the membrane protein tested here.

Recently new types of loops made of 25 µm Mylar foil with inner diameters ranging from 40 µm to 1 mm have been put on the market by Molecular Dimensions. Their advantage is the low background X-ray scattering. As this design is close to that used with the spatula technique described above, it might well facilitate future experiments of soft X-ray diffraction from protein crystals and in particular it might make the mounting procedure easier.

Clearly, further progress in the preservation of protein crystals while minimizing their protective solvent layer is necessary. The present result shown in Fig. 10 could be considerably improved by taking into account the protocol of crystal mounting developed at HASYLAB (Stuhrmann *et al.*, 1997) and making use of plastic loops.

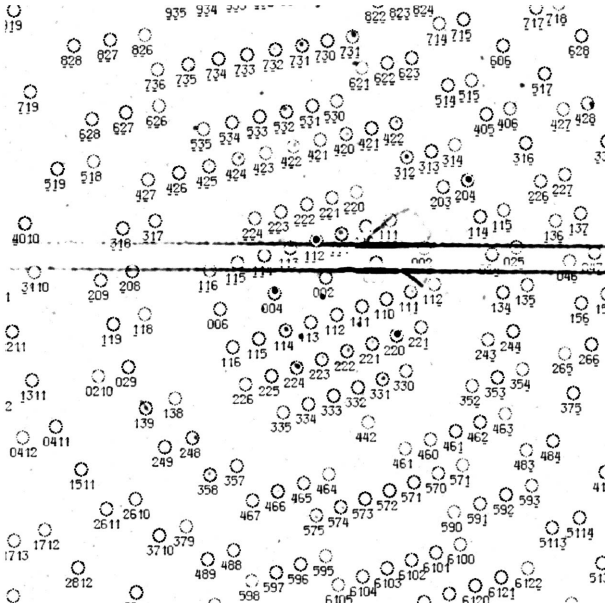

Figure 10
X-ray diffraction from an ADP/ATP carrier protein at $\lambda = 5.76$ Å. The crystal was rotated by 5° during a 30 min exposure. Most of the observed diffraction peaks can be explained by the predicted peak positions (circles). Other reflections appear to emerge from other parts of the bent crystal. As the intensity distribution recorded on the image plate has been filtered with a mask, the beam stop (horizontal rod) is presented by its contour lines.

6. Conclusion

The ancillary set-up for soft X-ray diffraction and spectroscopy, consisting of a helium box with its sample transfer line from IBS, a cold helium gas supply developed by EMBL and detectors provided by ESRF, has been shown to work reliably. Further improvements concern the shielding of the cold helium atmosphere in order to avoid the formation of frost.

The experience gained with this prototype helium box promotes ideas on further improvements. These mainly concern the shape of the box, which can now be optimized as some constraints given by the diffractometer of beamline ID01 do not exist any more. The range of scattering angles can be extended to the range −125° to +150° in the plane orthogonal to the cylinder axis and to ±62° in the plane of the cylinder axis. Moreover, the cold Mylar window did not withstand very well frequent changes of the image plate owing to formation of frost. A double window filled with warm helium circulating in a closed cycle is preferable.

The design of a new helium box for ID01 of ESRF is shown in Fig. 11. The large scattering angles corresponding to high structural resolution may be reached with soft X-ray diffraction from proteins (Stuhrmann *et al.*, 1997). The enlarged solid angle will certainly be useful in soft X-ray diffraction from crystals of low-molecular-weight compounds. The absorption corrections of the diffracted intensities require that data be taken at short X-ray wavelengths where absorption becomes negligible (Stuhrmann *et al.*, 1997).

While the diffraction intensity data at wavelengths near the *K*-edge of phosphorus can be obtained accurately from

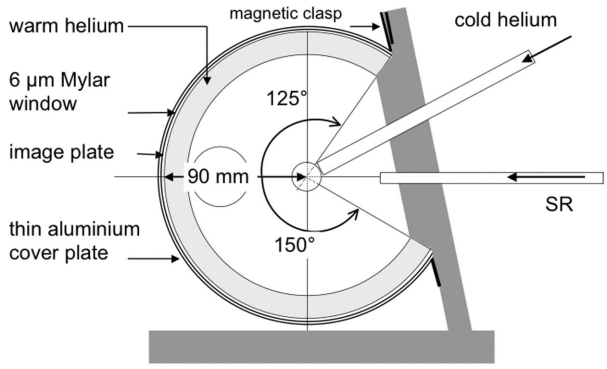

Figure 11
Helium box: the new design. The maximum polar angles are ±63°. A double window filled with warm helium replaces the Mylar window shown in Fig. 1, in order to avoid the formation of frost at the outer surface of this window. The second Mylar window, of thickness 6 µm, would decrease the transmission by almost 30% at wavelengths near the *K*-edge of phosphorus.

samples that tolerate an evacuated environment, *e.g.* purple membrane like many other materials to a good extent does, protein crystals lend themselves to soft X-ray diffraction less easily. The surface of a protein crystal needs to be watched more closely. The results of these explorative studies, which need the intense soft X-ray spectrum available only at synchrotron radiation sources, would be beneficial for conventional cryo protein crystallography as well. Finally, fluorescence measurements on a protein solution showed that it was possible to carry out studies on a relatively dilute sample.

Once the technique has come of age (Ren *et al.*, 1999), applications will be numerous. Phosphorus is present in all living systems at concentration levels that make it a useful label both in high- and low-resolution structure determination. The preference may be on the lower resolution side, as experiments near the *K*-edge of phosphorus limit the structural resolution to 2.88 Å. In a low-resolution map, the six phosphorus atoms of three cardiolipids and those of the three phopholipids per monomer carrier protein could easily be identified as they give rise to a relative change of the structure factor characterized by $R = 14\%$. Anomalous diffraction from phosphorus in RNA or DNA would provide valuable structural information on nucleoproteins like viruses and phages, not to mention on the interaction of lipids with membrane proteins.

References

Belrhali, H., Nollert, P., Royant, A., Menzel, C., Rosenbusch, J.-P., Landau, E. M. & Pebay-Peyroula, E. (1999). *Structure*, **7**, 909–917.
Carpentier, P., Bösecke, P., Bois, J.-M., Chesne, M.-L., Fanchon, E., Kahn, R., Stuhrmann, H. B. & Vicat, J. (2002). *Acta Phys. Pol.* **101**, 603–612.
Chabre, M., Cone, R. & Saibil, H. (2003). *Nature (London)*, **426**, 30–31.
Chesne, M.-L. (2002). Thesis, University Joseph-Fourier, Grenoble, France.

Djinović Carugo, K., Helliwell, J. R., Stuhrmann, H. B. & Weiss, M. S. (2005). *J. Synchrotron Rad.* **12**, 410–419.
George, G. N., Pickering, I. J., Via, G. H., Prince, R. C. & Sansone, M. (1993). *SSRL Activity Report 1993*, pp. 314–315. Stanford Synchrotron Radiation Laboratory, CA, USA.
Henderson, R., Baldwin, J. M., Ceska, T. A., Zemlin, F., Beckmann, E. & Downing, K. H. (1990). *J. Mol. Biol.* **213**, 899–929.
Henderson, R. & Unwin, P. N. T. (1975). *Nature (London)*, **257**, 28–31.
Henke, B. L., Gullikson, E. M. & Davis J. C. (1993). *Atom. Data Nucl. Data Tables*, **54**, 181–342.
Hütsch, M. (1992). Thesis, University of Hamburg, Germany.
Ito, A., Matsuda, H., Kitajima, Y. & Shinohara, K. (2003). *J. Phys. IV Fr.* **104**, 297–300.
Ito, A., Shinohara, K., Mizukami, Y., Nakano, H., Yada, K., Uehara, T. & Honda, T. (1998). *J. Synchrotron Rad.* **5**, 1099–1101.
Jost, P. C., MacMillen, D. A., Morgan, W. D. & Stoeckenius, W. (1978). *Light Transducing Membranes, Structure, Function and Evolution*, edited by D. W. Deamer, pp. 141–155. New York/San Francisco/ London: Academic.
Lehmann, M. S., Müller, H.-H. & Stuhrmann, H. B. (1993). *Acta Cryst.* D**49**, 308–310.
Munk, B. (1988*a*). Personal communication.
Munk, B. (1988*b*). Thesis, University of Hamburg, Germany.
Pebay-Peyroula, E., Dahout-Gonzales, C., Kahn, R., Trézéguet, V., Lauquin, G. J.-M. & Brandolin, G. (2003). *Nature (London)*, **426**, 39–44.
Ren, Z., Bourgeois, D., Helliwell, J. R., Moffat, K., Srajer, V. & Stoddard, B. L. (1999). *J. Synchrotron Rad.* **6**, 891–917.
Saibil, H., Chabre, M. & Worcester, D. L. (1976). *Nature (London)*, **262**, 266–270.
Seiff, F., Wallat, I., Ermann, P. & Heyn, M. P. (1985). *Proc. Natl. Acad. Sci. USA*, **82**, 3227–3231.
Stuhrmann, H. B. (1994). *Synchrotron Radiation in the Biosciences*, edited by S. Ebashi, D. T. Goodhead, J. R. Helliwell, H. E. Huxley, T. Iizuka, J. Kirz, T. Mitsui, E. Rubenstein, N. Sakabe, H. B. Stuhrmann, K. Wüthrich and G. Zaccai, pp. 119–138. Oxford: Clarendon.
Stuhrmann, H. B., Goerigk, G. & Munk, B. (1991). *Handbook on Synchrotron Radiation*, Vol. 4, edited by S. Ebashi, M. Koch and E. Rubenstein, pp. 555–580. Oxford: Elsevier Science.
Stuhrmann, S., Bartels, K. S., Braunwarth, W., Doose, R., Dauvergne, F., Gabriel, A., Knöchel, A., Marmotti, M., Stuhrmann, H. B., Trame, C. & Lehmann, M. S. (1997). *J. Synchrotron Rad.* **4**, 298–310.
Stuhrmann, S., Hütsch, M., Trame, C., Thomas, J. & Stuhrmann, H. B. (1995). *J. Synchrotron Rad.* **2**, 83–86.
Thomazeau, K., Curien, G., Dumas, R. & Biou, V. (2001). *Protein Sci.* **10**, 638–648.
Worcester, D. L. (1975). *Brookhaven Symposium on Neutrons in Biology*, Vol. III, pp. 37–57. Brookhaven National Laboratory, Upton, NY, USA.
Zaccai, G. & Gilmore, D. J. (1979). *J. Mol. Biol.* **132**, 181–191.